Steady State and Dynamic Simulation of a Small-Scale Hollow Fiber Membrane Humidifier

Markus Pollak[1] Manuel Kutz[2] Christian Schulze[2] Wilhelm Tegethoff[1,2] Jürgen Köhler[1]

[1]Institut für Thermodynamik, Technische Universität Braunschweig, Germany, {m.pollak, w.tegethoff, juergen.koehler}@tu-braunschweig.de
[2]TLK-Thermo GmbH, Germany, {m.kutz, c.schulze}@tlk-thermo.com

Abstract

Membrane humidifiers are commonly used in mobile proton exchange membrane (PEM) fuel cell systems to humidify the fuel cell supply air with the purpose of preventing the fuel cell membrane from drying out. In this paper, a humidifier model based on the number of transfer units (NTU) approach is set-up in Modelica, calibrated and validated using measurements of a test rig. The mass transfer model of our humidifier model is extended with a first order transfer function to capture dynamic operation. In a first step, the model is evaluated for steady state operating conditions. Second, the developed membrane humidifier model is simulated with dynamically changing operating conditions that are typical for mobile applications. Those simulation results are then compared to measurements. The aim of our study is to evaluate the accuracy of the humidifier model under various operating scenarios. Our results indicate that the NTU model is suitable to predict the water transfer under steady and dynamically changing operating conditions with low deviations to measurements.

Keywords: membrane humidifier, dynamic simulation, NTU, PEM fuel cell

1 Introduction

To ensure a high efficiency and a long lifetime of a Proton Exchange Membrane (PEM) fuel cell it is necessary to keep the membrane hydrated (Brandau, Heinke, and Koehler 2016; Ozen, Timurkutluk, and Altinisik 2016; Wu et al. 2020). This goal can be achieved by humidifying the supply air of the fuel cell. For this purpose, a membrane humidifier that transfers water along a concentration gradient from the wet fuel cell exhaust gas to the supply air can be used (Brandau, Heinke, and Koehler 2016). Alternative humidification methods are discussed in the literature but membrane humidifiers are considered a well-suited solution for the humidification of PEM fuel cells (Chen, Li, and Peng 2008). In automotive applications the operating conditions of such membrane humidifiers vary dynamically. Most of the studies in the literature focus on steady state operating conditions when assessing membrane humidifiers, e.g. (Cahalan et al. 2017; Nguyen, Vu, and Yu 2021; Pollak et al. 2023). A previous study (Pollak et al. 2023) investigated the same type of humidifier as discussed in our work, but focuses on detailed CFD model that is not suitable for system simulations with transient operation due to its long calculation times. Only few studies discuss transient operation of membrane humidifiers (Chen, Li, and Peng 2008; Park, Choe, and Choi 2008; Yun et al. 2018; Vu, Nguyen, and Yu 2022). Three of them do not compare their simulation results to experimental data (Park, Choe, and Choi 2008; Yun et al. 2018; Vu, Nguyen, and Yu 2022) and the fourth uses liquid water instead of a wet air flow as humidity source (Chen, Li, and Peng 2008).

The first aim of our study is to fill the existing gap of measurement data for the validation of transient operation. Moreover, we use our data to analyze if an NTU model is suitable to represent the dynamic operation accurately. Therefore, we first set up a model of a hollow fiber humidifier in Modelica based on the NTU method for mass exchangers as proposed by Brandau et al. (Brandau, Heinke, and Koehler 2016) and extend this approach with a first order transfer function in the mass transfer model. The purpose of the introduced first order transfer function is on the one hand to describe the dynamics of mass transfer and on the other hand to break potential non-linear systems in the mass transfer model. We use measurement data from a test rig to calibrate and validate the model for steady state and transient operating conditions. Furthermore, the calibration results of the model are compared to the results of a computational fluid dynamics (CFD) model of the same humidifier that was developed in a previous study (Pollak et al. 2023). The motivation for using Modelica to develop the humidifier model is the possibility to describe the humidifier model in an object-oriented way. This allows essential aspects such as the calculation of the mass transfer coefficient or the NTU characteristic to be described and modified as a replaceable submodel. This results in a high flexibility of the model, while the model code remains lean and understandable. A further advantage is that the governing physical laws can be written as equations in Modelica with variables whose physical units can be easily defined and checked. Moreover, the developed humidifier model integrates well into system simulation models with various operating conditions like PEM fuel cell systems.

The structure of our paper is as follows. In the following section, the working principle and the main features of the hollow fiber humidifier are introduced. Next, the test rig used for the measurements is presented. The third section discusses the modeling of the humidifier. It is followed by a section focusing on the steady state and dynamic simulation results.

2 Measurement of Hollow Fiber Humidifier

In this section, the general working principle of a mass exchanger is described. Moreover, the geometry of the investigated humidifier is introduced and its main features are presented. Second, the configuration of the test rig and the measured quantities are explained briefly.

2.1 Working principle

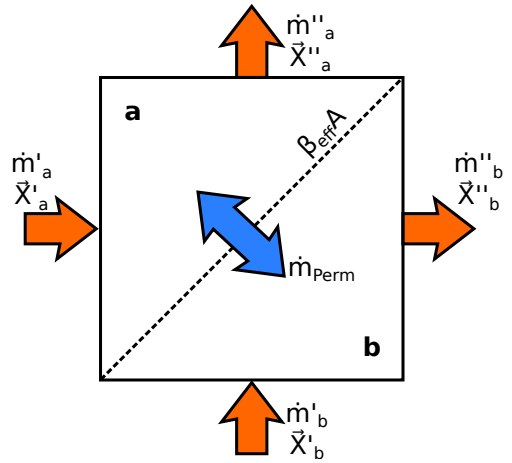

Figure 1. Sketch of a general mass exchanger that transfers mass from one stream to another. The vector $\vec{X}$ represents the state of the fluid at the depicted locations.

In this study, the hollow fiber membrane humidifier is investigated as special type of a mass exchanger. A sketch showing the most important quantities of such a mass exchanger is depicted in Fig. 1. All inlet quantities are denoted by $\square'$ whereas outlet values are marked as $\square''$. Typically, two mass flows enter a membrane humidifier. Both mass flow rates are altered due to the vapor transfer taking place inside the humidifier. Finally, two mass flows leave the mass exchanger. The mass transfer inside the mass exchanger is driven by a concentration difference according to Fick's Law. An effective mass transfer coefficient $\beta_{\text{eff}}A$ describes the ability of a device to transfer certain species. The mass transfer coefficient depends on the geometry, the used materials and the state of the depicted fluid flows (cf. Fig. 1). In a membrane humidifier a semipermeable membrane is used that poses a low resistance to water transfer but a high resistance to the transfer of other species. Depending on the inlet concentrations, the mass transfer can either occur from side A to B or from B to A. To achieve high water transfer rates membrane humidifiers are typically operated in counter- or crossflow arrangement.

2.2 Description of the Hollow Fiber Membrane Humidifier

In Fig. 2 a sketch of a hollow fiber humidifier geometry is shown. Only 12 fibers are depicted in Fig. 2 to highlight the geometric features and flow situation. As shown in Fig. 2, we investigate a counterflow arrangement of wet and dry air flows. As depicted in Figure 2, the wet air stream flows through the fibers, whereas the dry stream is fed to the shell. As a result of the manufacturing process, the fibers are placed randomly inside the shell. The

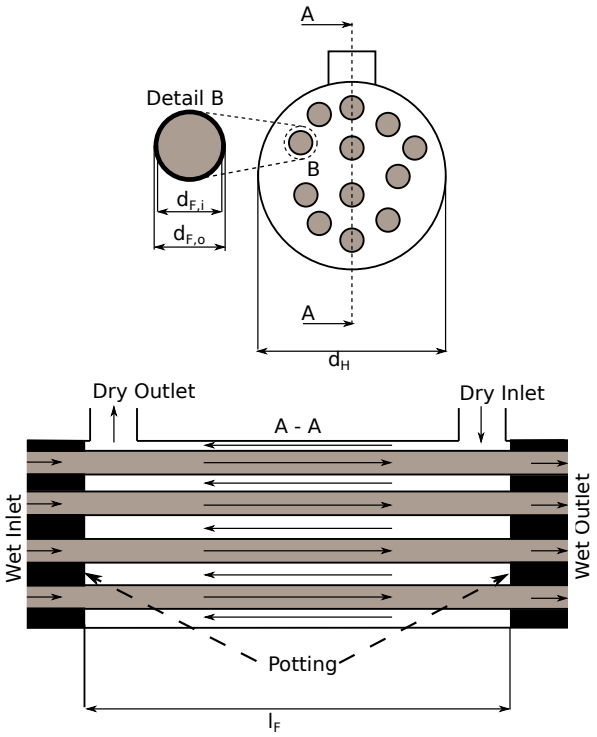

Figure 2. Geometric features of the modeled hollow fiber humidifier. The fibers are shown in light gray and the shell side with white background. The humidifier operates in counterflow, as seen in cut view A-A. A detailed view of a fiber is given in detail view B. Adopted from (Pollak et al. 2023)

investigated humidifier is available from the company Fumatech (FUMATECH BWT GmbH 2019) and was investigated using a CFD model and simulation in a previous study (Pollak et al. 2023). The material of the hollow fiber membranes is undisclosed by the manufacturer (Pollak et al. 2023). The relevant geometrical data of the fibers and the housing are given in Table 1.

2.3 Description of the Test Rig

The test rig is used to investigate the mass transfer of membrane humidifiers at various operating conditions. On the test rig, the same boundary conditions as in the simulation can be varied in their respective limits as described for the model (see Section 2.4).

Table 1. Parameters of the investigated hollow fiber membrane humidifier geometry.

Quantity	Symbol	Unit	Value
Number of fibers	n_F	1	488
Fiber outer diameter	$d_{F,o}$	mm	1
Fiber inner diameter	$d_{F,i}$	mm	0.9
Fiber length	l_F	mm	150.8
Housing inner diameter	d_H	mm	39.2

The water transfer is calculated using either sensor values of the dry side:

$$\dot{m}_{\mathrm{H2O,dry,perm}} = \dot{m}''_{\mathrm{dry}}\xi''_{\mathrm{H2O,dry}} - \dot{m}'_{\mathrm{dry}}\xi'_{\mathrm{H2O,dry}} \quad (1)$$

or using the sensors used on the wet side:

$$\dot{m}_{\mathrm{H2O,wet,perm}} = \dot{m}'_{\mathrm{wet}}\xi'_{\mathrm{H2O,wet}} - \dot{m}''_{\mathrm{wet}}\xi''_{\mathrm{H2O,wet}} \quad (2)$$

A steady-state operating point is only considered when the water transfer rates of wet and dry side match within a tolerance of 5 %. For calibration and validation of the models, both results are averaged.

A P&ID showing the humidifier test rig can be found in Figure 3. The sensors used in our test rig and their respective uncertainties are given in Table 2. Based on those uncertainties the error propagation is calculated according to the guideline (Joint Committee for Guides in Metrology (JCGM) 2008).

Air is fed to the test rig from a pressurized air storage tank. Behind the air storage, the air flow is split into two streams: one for the wet and one for the dry side. The wet path simulates the exhaust gas from the fuel cell and the dry path the air supplied to the humidifier. A control valve at the inlet of each path is used to adjust each the wet and dry air mass flow rates, respectively. Next, both air streams are heated up by electrical heaters to reach an operating temperature typical for membrane humidifiers used in PEM fuel cell systems. The pressure of both streams can be controlled individually by two valves located at the outlet of the air paths. Vapor is fed from a vapor storage tank through a controlled valve to achieve the desired inlet humidity of the wet air stream. The tubes of the vapor supply line are heated to avoid condensation, which is required to get valid measurement results. The availability of heaters on all tubes is important because the humidity sensors installed can only measure water in gaseous form and therefore condensation has to be prohibited. If condensation of water occurs, the water transfer rates measured on the dry and wet side deviate from each other. Thus, the water transfer rates are continuously checked during the measurement.

2.4 Inputs and Parameters

The water transfer in the humidifier is governed by the inlet conditions of the wet and dry flow and the mass transfer capability. To mimic the operation in a fuel cell system, the following quantities can be adjusted:

- mass flow rates of both, dry and wet, streams;
- temperatures of both, dry and wet, streams;
- pressures of both, dry and wet, streams;
- relative humidity of the wet stream.

The parameter limits for the boundary conditions are listed in Tab. 3. Since both mass flows are conditioned to have nearly same temperature and the humidifier is isolated against the environment, heat transfer is considered to be of negligible effect.

Since the membrane permeability is not disclosed by the manufacturer it is considered to be a calibration parameter of the humidifier model that must be identified by a calibration process using the measurement data. This calibration result is than compared to a fitting result of a previous study that used a CFD model (Pollak et al. 2023).

3 NTU Membrane Humidifier Model for System Simulations

The humidifier models discussed in this study are set-up using the commercially available Modelica libraries TIL, TILMedia and the TIL3_Addon_HydrogenEnergySystems each in version 3.13.0 (TLK-Thermo GmbH 2022). Dymola 2023x is used as modeling and simulation environment (Dassault Systèmes SE 2022a). A novelty of our approach is to use a first order transfer function in the mass transfer model. The introduction of a first order transfer function for the permeating mass is motivated on the one hand numerically and on the other hand physically. A numerical benefit of the introduced state is that non-linear systems can be eliminated. From a physical perspective the first order transfer function can be used to reflect the dynamics of the mass transfer, which is commonly disregarded in mass exchanger models.

3.1 NTU Humidifier Model

The developed humidifier model is built upon the NTU approach as derived by Brandau et al. (Brandau, Heinke, and Koehler 2016) and derived from the class available in TIL3_Addon_HydrogenEnergySystems (TLK-Thermo GmbH 2022).

An overview of the humidifier model with its replaceable submodels and records, the used ports and the objects for thermophysical property calculations is displayed in Fig. 4. The model consist of two air paths (a and b). Both paths are separated by the membrane that is visualized as a dashed line in Fig. 4. Path a is connected to the outside by two connectors, A_a and B_a. Just like path a, path b has two connections to the outside A_b and B_b. The model can handle flow from port A to B and vice versa in both paths. At each port a gas object is located (cf. Fig. 4) that is used to calculate the thermophysical properties of the gas mixture at the ports. In both paths a replaceable model for the pressure drop is applied. Since no pressure drop Δp is

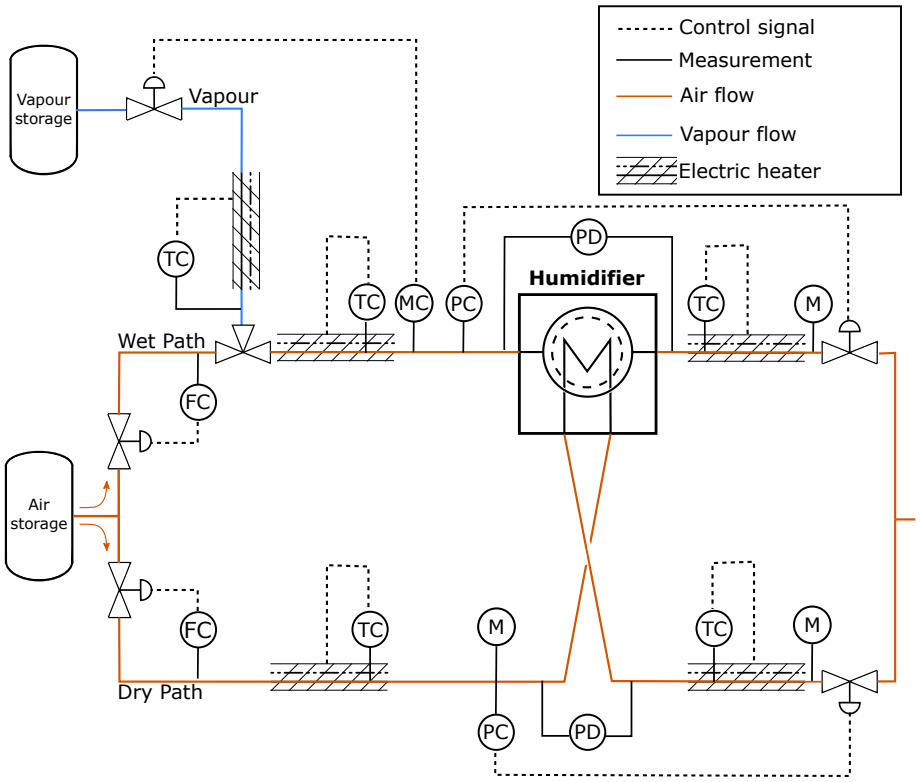

Figure 3. Piping and instrumentation diagram of the test rig used for the investigation of the water permeation in the hollow fiber membrane humidifier at various inlet conditions (Pollak et al. 2023). Flow (F), temperature (T), moisture (M) and pressure (P) sensors are installed. Control variables are marked by a 'C'. Pressure difference measurements are marked with a 'PD'.

Table 2. Used sensors and their measurement uncertainties.

Sensor	**Measured Quantity**	**Output Unit**	**Uncertainty**
Vaisala HMT-337	Humidity	%	$\pm(1.5+0.015\varphi)$
Omega FMA-1609A	Mass flow rate	g/s	$\pm(0.008\dot{m}+0.00204)$
Omega PXM459	Differential pressure	Pa	± 56
WIKA P-30	Pressure	bar	± 0.068
WIKA TR-40	Temperature	K	$\pm 0.15+0.002(T-273.15)$

Table 3. Limits of the boundary conditions for simulation and measurement of the membrane humidifier. The values of water mass fraction apply to the wet side only.

Parameter	Minimum	Maximum
Temperature	60 °C	80 °C
Pressure	1.5 bar	2.0 bar
Air flow rate	0.2 g/s	0.7 g/s
Water mass fraction	0.027	0.172

investigated in our study, the pressure drop is set to zero. The same is true for the heat transfer, therefore the heat transfer coefficient α is also set to zero. The calculation of the overall mass transfer coefficient β_{eff} is discussed in Sec 3.2. In the top right of Fig. 4 a record storing the geometry information of the humidifier is depicted.

The NTU approach for mass exchangers is formulated in analogy to the well known NTU approach for heat exchangers (Brandau, Heinke, and Koehler 2016). Three dimensionless numbers are derived from the inlet quantities given in Fig. 1 to describe the mass transfer between two fluid flows in the NTU model. The three dimensionless numbers described by Brandau et al. (Brandau, Heinke, and Koehler 2016) are the mass transfer efficiency, the ratio of volume flow rates and the number of transfer units. These three dimensionless numbers can be formulated for the dry and wet side of the humidifier, respectively. To calculate the results, only one set of the three dimensionless numbers must be calculated and is denoted by the subscript a in the following. The first dimensionless number is the mass transfer efficiency:

$$\eta_a = \frac{c''_{a,\text{H2O}} - c'_{a,\text{H2O}}}{c'_{b,\text{H2O}} - c'_{a,\text{H2O}}} \tag{3}$$

It describes the ratio of actual mass transfer to the theoretically possible mass transfer. Additionally, the ratio of

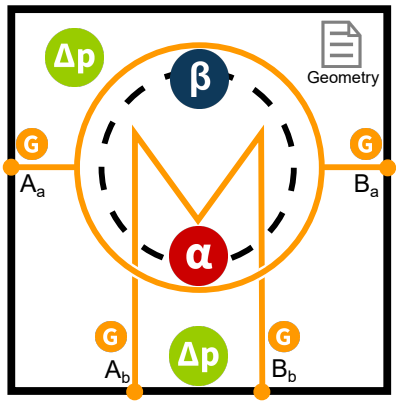

Figure 4. Overview of the humidifier model with submodels, ports and objects for property calculations.

volume flow rates is required:

$$VFR_a = \frac{\dot{V}'_a}{\dot{V}'_b} \tag{4}$$

Finally, the Number of Transfer Units (NTU) can be defined:

$$NTU_a = \frac{\beta_{\text{eff}} A}{\dot{V}_a} \tag{5}$$

To achieve high mass transfer efficiencies, the humidifier operates in counterflow. The following equations derived by Brandau, Heinke, and Koehler (2016) are used to calculate the mass transfer efficiency:

$$\eta_a = \begin{cases} \frac{NTU_a}{1+NTU_a}, & \text{if } VFR_a = 1 \\ \frac{1-exp[(VFR_a-1)NTU_a]}{1-VFR_a\,exp[(VFR_a-1)NTU_a]}, & \text{otherwise} \end{cases} \tag{6}$$

The transferred water is than calculated based on the mass transfer efficiency and the inlet quantities:

$$\dot{m}_{perm,H2O} = M_{H2O}\eta_a(c'_{b,H2O} - c'_{a,H2O})\dot{V}'_a \tag{7}$$

In order to allow a fitting of the suggested model to transient data and to break non-linear systems, a first order transfer function is introduced that can be selected by the user (TLK-Thermo GmbH 2022). The mass transfer dynamics are caused by a combination of effects i.e. sensor delay and the residence time of supplied water in the humidifier. In our approach, the ratio of permeation rate and the smaller air mass flow rate at a given time is introduced as state variable:

$$\Xi = \frac{\dot{m}_{\text{perm,H2O}}}{min(\dot{m}'_a, \dot{m}'_b)} \tag{8}$$

Ξ_{state} is introduced as state variable as motivated above to describe the dynamics of the mass transfer process defined by the equation

$$\frac{d\Xi_{\text{state}}}{dt} = \frac{\Xi - \Xi_{\text{state}}}{\tau_{\text{perm}}} \tag{9}$$

The permeation rate $\dot{m}_{perm,H2O,state}$ that includes the introduced dynamics is than calculated using the following equation:

$$\dot{m}_{\text{perm,H2O,state}} = \begin{cases} \Xi_{\text{state}}\dot{m}'_a & \text{if } \dot{m}'_b \geq \dot{m}_a \\ \Xi_{\text{state}}\dot{m}'_b & \text{otherwise} \end{cases} \tag{10}$$

The advantage of using Ξ_{state} instead of a state for the permeation rate $\dot{m}_{\text{perm,H2O}}$ is that Ξ_{state} is not directly linked to the inflowing mass flow rate $\dot{m}'_a$, but takes both air mass flow rates into account. It is linked to the smaller mass flow rate $min(\dot{m}_a, \dot{m}_b)$ so that the permeation rate cannot exceed the capacity of the smaller mass flow. Thus, the model becomes more robust. This is especially important for dynamic changes, e.g. when one of the mass flow rates is decreased dramatically.

If no first order transfer function is used, the following equation holds:

$$\dot{m}_{\text{perm,H2O,state}} = \dot{m}_{\text{perm,H2O}} \tag{11}$$

The calculated permeation rate is than introduced in the balance equations for mass and species. Those balance equations are formulated separately for each path. The mass balances of both paths are connected with the permeation rate and read:

$$\dot{m}''_a = \dot{m}'_a - \dot{m}_{\text{perm,H2O,state}} \tag{12}$$
$$\dot{m}''_b = \dot{m}'_b + \dot{m}_{\text{perm,H2O,state}} \tag{13}$$

Furthermore, the water balances for both paths read:

$$\dot{m}''_{a,\text{H2O}} = \dot{m}'_{a,\text{H2O}} - \dot{m}_{\text{perm,H2O,state}} \tag{14}$$
$$\dot{m}''_{b,\text{H2O}} = \dot{m}''_{b,\text{H2O}} + \dot{m}_{\text{perm,H2O,state}} \tag{15}$$

The mass transfer is accompanied by an enthalpy flow that is calculated using the inlet states and the previously discussed permeation rate:

$$\dot{H}_{\text{perm}} = \begin{cases} \dot{m}_{\text{perm,H2O,state}}\, h_a & \text{if } c'_{a,\text{H2O}} \geq c'_{b,\text{H2O}} \\ \dot{m}_{\text{perm,H2O,state}}\, h_b & \text{otherwise} \end{cases} \tag{16}$$

The enthalpy flow rate of the permeation flow is included in the energy balance equation of both paths:

$$\dot{H}''_a = \dot{H}'_a - \dot{H}_{\text{perm}} \tag{17}$$
$$\dot{H}''_b = \dot{H}'_b + \dot{H}_{\text{perm}} \tag{18}$$

Furthermore, a heat transfer rate can be calculated in the model, too, but is not discussed here due to the selection of nearly isothermal operating conditions.

3.2 Mass Transfer in the Membrane Humidifier

To calculate the NTU in the presented model, the overall mass transfer coefficient is required. The calculation of this mass transfer coefficient takes place in a submodel, which can easily be replaced and adapted. In general, the effective mass transfer coefficient is the reciprocal of the overall mass transfer resistance:

$$\beta_{\text{eff}} A = \frac{1}{R_{\text{eff}}} \tag{19}$$

This effective mass transfer resistance can be split in three parts that are connected in series as given in:

$$R_{\text{eff}} = R_{\text{conv,wet}} + R_{\text{mem}} + R_{\text{conv,dry}} \tag{20}$$

The first term on the right-hand side describes the convective resistance to the mass transfer in the wet flow. Second, the membrane poses a resistance to the mass transfer. This membrane resistance is much lower for vapor than for other gas components. Therefore, we assume that only vapor is transferred in the humidifier. Last, another convective resistance is present on the dry side.

Both convective resistances are calculated using Sherwood correlations that were empirically determined in the literature (Costello et al. 1993; Gnielinski 2010). Using the determined Sherwood numbers, the mass transfer coefficients for the convective transfer can be calculated:

$$\beta_i = \frac{Sh D_{\text{H2O,Air}}}{l_{ch}} \tag{21}$$

For the calculation of the Sherwood number of wet air flow inside the fibers, the well known correlations for heat transfer in tube are adapted from Gnielinski (2010):

$$Sh_{\text{wet}} = [Sh_{\text{wet,1}}^3 + 0.7^3 + ([Sh_{\text{wet,2}} - 0.7)^3]^{1/3} \tag{22}$$

$$Sh_{\text{wet,1}} = 3.66 \tag{23}$$

$$Sh_{\text{wet,2}} = 1.615 \left(Re\, Sc \frac{d_{hyd}}{l_F} \right)^{1/3} \tag{24}$$

The hydraulic diameter equals the inner diameter of a single fiber. On the other hand, the shell side is more complicated due to more complex flow phenomena. Costello et al. (1993) proposed the following correlation that includes the packing density Φ :

$$Sh_{\text{dry}} = (0.53 - 0.58\Phi) Re^{0.53} Sc^{0.33} \tag{25}$$

This correlation is also used by Vu, Nguyen, and Yu (2022) to model the shell side convective mass transfer of a hollow fiber humidifier. The packing density is defined as ratio of shell cross sectional area to the cross sectional area occupied by the fibers:

$$\Phi = \frac{n_F d_{F,o}^2}{d_H^2} \tag{26}$$

The mass transfer resistance of the membrane is modeled with a constant diffusion coefficient and the thickness given in Tab. 1:

$$R_{\text{mem}} = \frac{\delta}{D_{\text{mem}} A_{\text{mem}}} \tag{27}$$

4 Calibration and Validation of the Humidifier Models

In this section, the calibration and validation of the presented model using measurements of the test rig are shown. At first, the membrane diffusion coefficient is calibrated and validated using steady state data of the humidifier reflecting the range of operating conditions (cf. Tab. 3). Next, the introduced time constant of mass transfer is calibrated using measurement data and the model with the previously calibrated mass transfer coefficient.

4.1 Steady State Operation

The available measurement data contains two data sets. Our first data set includes 105 steady state operating points. For this data set the volume flow rate ratio was kept close to one ($VFR \approx 1$). The points of this first data set are randomly split between the calibration and the validation set. We use 60 % of the data for the calibration and 40 % for the validation of the model. The second data set is used for validation only. It contains only eight points but in contrast to the operating points the ratio of volume flow rates differs significantly from one. With this data set the accuracy of the NTU model when predicting water transfer rates at operating points very different from the calibration data is assessed. The calibration of the model is done using the truncated Newton (TNC) optimization method of the SciPy library written in Python (Virtanen et al. 2020). For the calibration process, the model is exported from Dymola as functional mock-up unit (FMU) and simulated in Python using FMPy (Dassault Systèmes SE 2022b). The root mean square error (RMSE) of the simulated $\hat{\dot{m}}_{\text{perm}}$ and measured water permeation rate $\dot{m}_{\text{perm}}$ is used as objective function to be minimized:

$$\text{RMSE} = \sqrt{\frac{\sum_{i=1}^{n} (\dot{m}_{\text{perm},i} - \hat{\dot{m}}_{\text{perm},i})^2}{n}} \tag{28}$$

The objective of the fitting process is to find the membrane diffusion coefficient $D_{\text{mem,fit}}$ that minimizes the previously defined RMSE of the model $\vec{X}_{a,b}$:

$$D_{\text{mem,fit}} = \text{argmin RMSE}(\vec{X}_{a,b}, D_{\text{mem}}) \tag{29}$$

Finally, the membrane diffusion coefficient for vapor $D_{\text{mem,fit}} = 3.63e-7\, m^2/s$ that minimizes the deviation of simulation and measurement is found. This fitting result is close to the value $D_{\text{mem,CFD}} = 4.02e-7\, m^2/s$, determined in a previous study where a smaller data set and a CFD

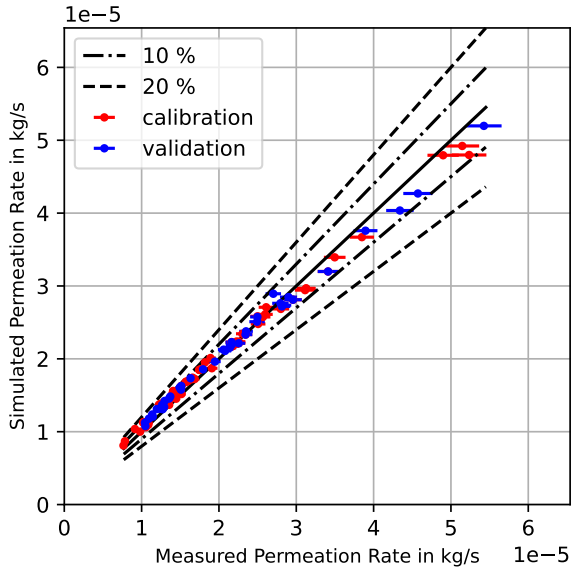

Figure 5. Comparison of the calibration and validation results of the NTU model with the steady state measurement data.

model of the same humidifier were investigated (Pollak et al. 2023). The simulation results of the calibrated model are shown in Fig. 5, marked by blue points. The depicted error bars represent the measurement uncertainty of permeation rate calculated according to the guideline (Joint Committee for Guides in Metrology (JCGM) 2008). For all investigated points, the deviation of the simulation is less than 20 % in comparison to the measurement. Moreover, the results of the validation are plotted in Fig. 5, too. Again, the deviation of the simulation results from the measurements is less than 20 % for the validation data. The deviation of the simulated from the measured permeation rate is less than 10 % for most operating points and often within the range of measurement uncertainty. In Tab. 4 an overview of the RMSE is presented. From the values shown in Tab. 4, only a small difference between calibration and validation can be identified.

Table 4. RMSE of the simulated and measured water permeation rate for calibration, validation and total data.

	Calibration	Validation	Total
RMSE in g/s	1.3242e-6	1.4036e-6	1.3560e-6

To test the capability of the NTU model to extrapolate, another data set is used. A special feature of this data set is that the ratio of volume flow rates is varied systematically from 0.37 to 2. To assess the model accuracy, the mass transfer efficiency of both measurement and simulation is plotted versus the NTU of the simulations in Fig. 6. One can see that the simulation results lie directly on the characteristic lines representing a fixed volume flow ratio. On the other hand, the measurement results do not directly match the characteristic lines, which is due to deviations of measurements and simulation results. Nonetheless, simulation results and measurements show a similar trend. Furthermore, the relative deviation of the simulated and measured mass transfer efficiencies is below 10 % for all considered operating points.

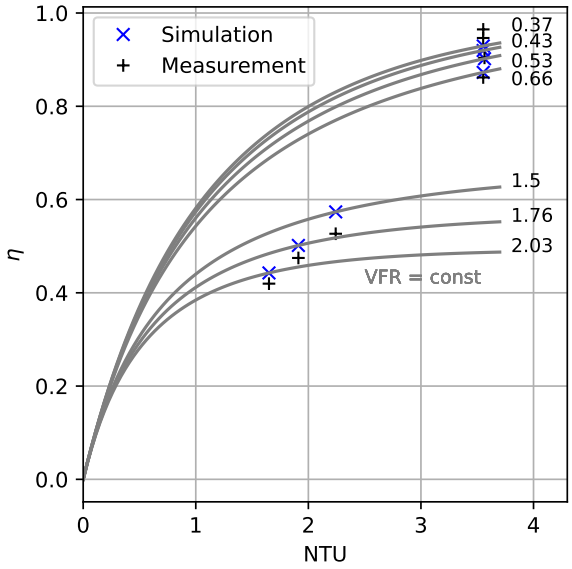

Figure 6. Comparison of simulation results and measurements on validation data for different volume flow rate ratios. The values of the investigated VFR_a are shown next to the lines.

In summary one can conclude that the developed NTU model can accurately predict the water permeation under various steady state operating conditions. The ability of the NTU model to extrapolate was demonstrated by using the NTU model that was calibrated for a $VFR_a \approx 1$, for a range of $0.35 < VFR_a < 2.0$.

4.2 Dynamic Simulations

Another goal of our study is to evaluate if the developed humidifier model is able to predict dynamic operation of the humidifier accurately. For this purpose, we use data from the test rig that was collected while switching from one operating point to another. Therefore, most of our investigations apply to the water mass fraction feed to the wet air inlet. To investigate the dynamics of the humidifier, the water mass fraction at the wet inlet was controlled manually to mimic a step response.

For the dynamic simulations we use time series data of a typical measurement session as input for the humidifier model. We extract the sensor values of the inlet quantities of the humidifier from the measurement data, described in Sec. 2.4, and feed those quantities to real input blocks of the humidifier model. The membrane permeability was kept at $D_{mem} = 3.63e-7 m^2/s$, as identified in the previous section.

In a first step, the time constant for the first order delay was calibrated manually to match the water diffusion over a period of 24000 s. The mean absolute error (MAE) was

used as metric to evaluate the calibration

$$\mathrm{MAE} = \frac{1}{n}\sum_{i=1}^{n} |\dot{m}_{\mathrm{perm},i} - \hat{\dot{m}}_{\mathrm{perm},i}| \tag{30}$$

That MAE was used in the following object function:

$$\tau_{\mathrm{perm,fit}} = \mathrm{argmin}\ \mathrm{MAE}(\vec{X}_{a,b}, \tau_{\mathrm{perm}}) \tag{31}$$

A value of $\tau_{\mathrm{perm,fit}} = 6.1\,\mathrm{s}$ was identified to yield the minimal absolute deviations between measurement and simulation results. At this point it shall be stated, that the dynamics of the measurements do not only originate from the humidifier itself but also from the time constants of the used sensors.

In Fig. 7 an exemplary step response of the water permeation rate caused by an abrupt decrease in the water mass fraction at the wet inlet from $\xi'_{H2O,wet} = 0.083$ to $\xi'_{H2O,wet} = 0$ is shown. All operating conditions of this scenario are given in Tab. 5. The measurement of the permeation rate is shown as a blue line. To show the influence of the introduced time constant, the humidifier model was simulated three times with differently parameterized values of 1.0 s, 6.1 s and 20 s for the time constant. In Fig. 7, it is obvious that a time constant of 20 s leads to a slow response and high deviations from the measurement. Furthermore, it can be observed that the green and blue line are close to each other. A minor deviation can be found in the last moments of the step response. In contrast, the model parameterized with a time constant of 1.0 s reacts too abruptly. Comparing the models to each other, one can see that all models predict the same steady state solution as expected and show a small deviation from the measurement.

Table 5. Boundary conditions before and after step shown in Fig. 7 used for the fitting of the time constant. Temperature and pressure apply to both sides.

Parameter	Before	After
Temperature	70 °C	70 °C
Pressure	1.5 bar	1.5 bar
Air flow rate, dry	0.3 g/s	0.3 g/s
Air flow rate, wet	0.65 g/s	0.6 g/s
Water mass fraction, wet	0.083	0.0

For the validation of the fitted time constant the data of another measurement session is used. Just as for calibration, a step response of the humidifier due to a change of water mass fraction at the wet inlet is also used for validation. The operating conditions are given in Tab. 6. In contrast to the calibration data, the focus lies on a step to higher water mass fractions. In Fig. 8 the measured and simulated water permeation rates are plotted over the time. One can easily identify that the dynamics of opening the vapor control valve are more complex than the closing when comparing Fig. 8 and Fig. 7. In Fig. 8 a first abrupt rise of the permeation rate is visible nearly instantly when

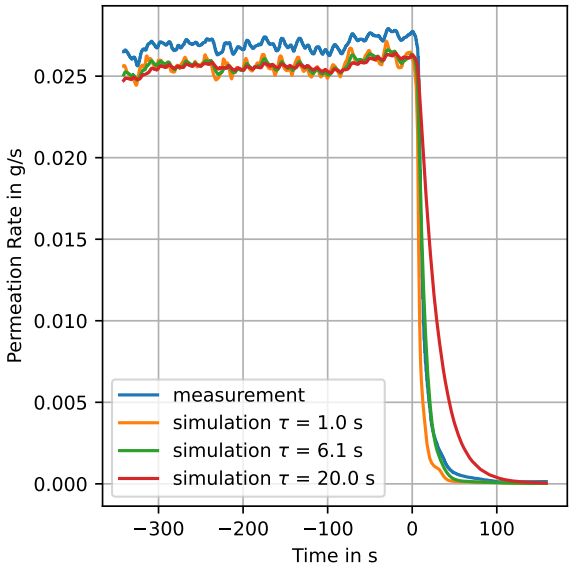

Figure 7. Comparison of the simulation results of differently parameterized NTU models with the measurement data of a step at t = 0 s to dry conditions. The NTU models use different time constants for the introduced first order behavior.

Table 6. Boundary conditions before and after step shown in Fig. 8 used for the validation of the fitted model. Temperature and pressure values apply to both sides.

Parameter	Before	After
Temperature	80 °C	80 °C
Pressure	2.0 bar	2.0 bar
Air flow rate, dry	0.4 g/s	0.4 g/s
Air flow rate, wet	0.4 g/s	0.43 g/s
Water mass fraction, wet	0.0	0.069

the vapor control valve is opened. This first rise is followed by a plateau with a duration of about 30 s. After this phase a less steep rise of the permeation rate is observed. Opening the steam valve affects both the control of the steam generator and storage tank as well as the control of the air supply. This is the reason for the complex dynamics when opening the valve. Again, the results of the three NTU models with different time constants are shown. The measure response of the humidifier depicted in Fig. 8 is accurately reproduced by the NTU model with the fitted time constant. The NTU model with the lowest time constant of 1 s shows an overshoot to the first part of the step, whereas the rising time of the NTU model with the highest time constant is way to long. As discussed for the fitting results, a slight deviation of the steady state results between measurement and all simulation models can be observed.

In summary, the developed model is suitable for dynamic simulations as well. It was shown that the model is able to reproduce the dynamics of the measured data accurately.

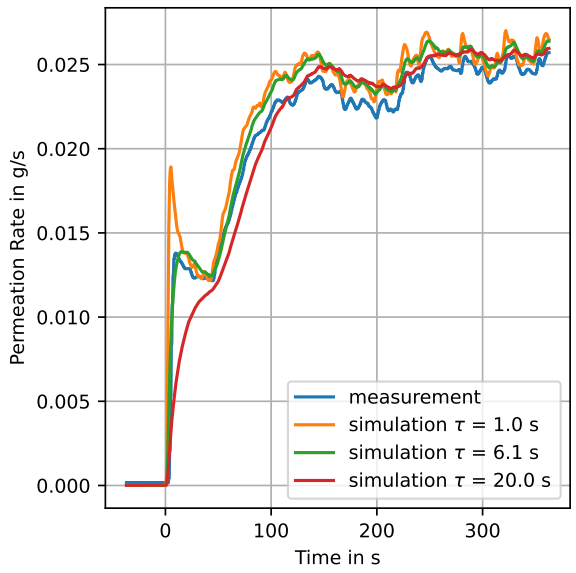

Figure 8. Comparison of the simulation results of differently parameterized NTU models with the measurement data of a step at t = 0 s from completely dry to wet conditions. The NTU models use different time constants for the introduced first order behavior.

4.3 Computational Times

The presented NTU humidifier model can be used for real-time predictions due to its fast computations resulting from the employed simple model structure. When the model is packaged into FMU format the simulation takes an average of 27.37 s computational time to simulate a full time series of 17428 s. The mean computational time to calculate a single time step of 1 s time is 0.00157 s. The calculations were done on an AMD Ryzen Threadripper 1900X.

5 Conclusion and Outlook

The results of our study show that the presented NTU model can accurately predict the water transfer occurring inside a hollow fiber humidifier under steady state as well as for dynamic operating. As a first result, the diffusion coefficient of water in the membrane was determined for the steady state operation. It was found that this fitting result agrees well with the results from a previous study (Pollak et al. 2023). In a next step, the model was fitted to dynamic measurement data while keeping the fitted value of the membrane diffusion coefficient. With the fitted model a validation step response can be predicted accurately. Furthermore, it was demonstrated that our developed model is capable of real time predictions on a desktop computer. For future studies, the effect of a simultaneously occurring heat transfer is an important topic to investigate. Another effect to be investigated in this context is the enthalpy of ad- and desorption of water on the membrane surfaces. Moreover, it should be assessed whether the humidifier model is able to capture the effects of liquid water on mass transfer as investigated by Mull et al. (2023) , that might be present in the exhaust gas of the fuel cell.

Acknowledgments

This work has been supported by both the German Federal Ministry of Education and Research and the German Federal Ministry of Economic Affairs and Climate Action as part of the projects AUTO-GEN (grant number 01IS20086B) and SKAiB (grant number 20M2101F).

Nomenclature

Abbreviations

CFD	Computational Fluid Dynamics
FMU	Functional Mock-up Unit
MAE	Mean absolute error
PEM	Proton Exchange Membrane
RMSE	Root Mean Square Error

Latin Symbols

A	Area, m^2
c	Concentration, $mol/(m^3)$
D	Diffusion coefficient, m^2/s
d	Diameter, m
h	Specific enthalpy, $W/(m^2K)$
$\dot{H}$	Enthalpy flow W
i	Number, *dimensionless*
l	Length, m
M	Molar mass, kg/mol
n	Number, *dimensionless*
NTU	Number of transfer units, dimensionless
$\dot{m}$	Mass flow rate, kg/s
p	Pressure, Pa
R	Mass transfer resistance, s/m^3
Re	Reynolds number, dimensionless
Sc	Schmidt Number, dimensionless
Sh	Sherwood Number, dimensionless
t	Time, s
T	Temperature, K
VFR	Ratio of volume flow rates, dimensionless
$\vec{X}$	State vector

Greek Symbols

β Mass transfer coefficient, m/s

δ Thickness, m

η Mass transfer efficiency dimensionless

ξ Mass fraction, kg/kg

Ξ Ratio of transferred water, kg/kg

τ Time constant, *s*

Φ Packing density, dimensionless

Subscript

a Side a

b Side b

ch Characteristic

conv Convective

eff Effective

fit Result of the calibration

H2O Water

hyd hydraulic

mem Membrane

perm Permeation

Superscript

$\square'$ inlet quantity

$\square''$ outlet quantity

References

Brandau, N., S. Heinke, and J. Koehler (2016-08). "Analysis of mass exchangers based on dimensionless numbers". en. In: *International Journal of Heat and Mass Transfer* 99, pp. 261–267. ISSN: 00179310. DOI: 10.1016/j.ijheatmasstransfer.2016.03.080.

Cahalan, T. et al. (2017). "Analysis of membranes used in external membrane humidification of PEM fuel cells". In: *International Journal of Hydrogen Energy* 42.22, pp. 15370–15384.

Chen, Dongmei, Wei Li, and Huei Peng (2008-05). "An experimental study and model validation of a membrane humidifier for PEM fuel cell humidification control". en. In: *Journal of Power Sources* 180.1, pp. 461–467. ISSN: 03787753. DOI: 10.1016/j.jpowsour.2008.02.055. URL: https://linkinghub.elsevier.com/retrieve/pii/S0378775308003625 (visited on 2023-05-03).

Costello, M.J. et al. (1993-06). "The effect of shell side hydrodynamics on the performance of axial flow hollow fibre modules". en. In: *Journal of Membrane Science* 80.1, pp. 1–11. ISSN: 03767388. DOI: 10.1016/0376-7388(93)85127-I. URL: https://linkinghub.elsevier.com/retrieve/pii/037673889385127I (visited on 2023-04-28).

Dassault Systèmes SE (2022a). *Dymola 2023x*. https://www.3ds.com/products-services/catia/products/dymola/.

Dassault Systèmes SE (2022b). *FMPy v0.3.12*. https://github.com/CATIA-Systems/FMPy.

FUMATECH BWT GmbH (2019). *ECOMATE Humidifiers*. URL: https://www.fumatech.com/.

Gnielinski, Volker (2010). "G1 heat transfer in pipe flow". In: *VDI heat atlas*. Springer, pp. 691–700.

Joint Committee for Guides in Metrology (JCGM) (2008-09). *Evaluation of measurement data — Guide to the expression of uncertainty in measurement*. Guideline.

Mull, Sophie et al. (2023-07). "Membrane humidifier model for PEM fuel cell systems". en. In: *European Fuel Cell Forum 2023*. Lucerne.

Nguyen, Xuan Linh, Hoang Nghia Vu, and Sangseok Yu (2021). "Parametric understanding of vapor transport of hollow fiber membranes for design of a membrane humidifier". In: *Renewable Energy* 177, pp. 1293–1307. ISSN: 0960-1481. DOI: https://doi.org/10.1016/j.renene.2021.06.003. URL: https://www.sciencedirect.com/science/article/pii/S0960148121008673.

Ozen, Dilek Nur, Bora Timurkutluk, and Kemal Altinisik (2016). "Effects of operation temperature and reactant gas humidity levels on performance of PEM fuel cells". In: *Renewable and Sustainable Energy Reviews* 59, pp. 1298–1306. ISSN: 1364-0321. DOI: https://doi.org/10.1016/j.rser.2016.01.040. URL: https://www.sciencedirect.com/science/article/pii/S1364032116000708.

Park, Sang-Kyun, Song-Yul Choe, and Seo-ho Choi (2008). "Dynamic modeling and analysis of a shell-and-tube type gas-to-gas membrane humidifier for PEM fuel cell applications". In: *International journal of hydrogen energy* 33.9, pp. 2273–2282.

Pollak, Markus et al. (2023). "Analysis of Surrogate Models for Vapour Transport and Distribution in a Hollow Fibre Membrane Humidifier". en. In: *Energies* 16.6. ISSN: 1996-1073. DOI: https://doi.org/10.3390/en16062578.

TLK-Thermo GmbH (2022). *TIL Suite*. https://www.tlk-thermo.com/index.php/de/software/til-suite.

Virtanen, Pauli et al. (2020). "SciPy 1.0: Fundamental Algorithms for Scientific Computing in Python". In: *Nature Methods* 17, pp. 261–272. DOI: 10.1038/s41592-019-0686-2.

Vu, Hoang Nghia, Xuan Linh Nguyen, and Sangseok Yu (2022). "A Lumped-Mass Model of Membrane Humidifier for PEMFC". In: *Energies* 15.6, p. 2113.

Wu, Di et al. (2020). "Review of system integration and control of proton exchange membrane fuel cells". In: *Electrochemical Energy Reviews* 3, pp. 466–505.

Yun, Sungho et al. (2018-10). "Numerical analysis on the dynamic response of a plate-and-frame membrane humidifier for PEMFC vehicles under various operating conditions". en. In: *Open Physics* 16.1, pp. 641–650. ISSN: 2391-5471. DOI: 10.1515/phys-2018-0081. URL: https://www.degruyter.com/document/doi/10.1515/phys-2018-0081/html.